NANO LETTERS

Letter

pubs.acs.org/NanoLett

Epitaxial Growth of Thin Ferroelectric Polymer Films on Graphene Layer for Fully Transparent and Flexible Nonvolatile Memory

Kang Lib Kim,[†] Wonho Lee,[‡] Sun Kak Hwang,[†] Se Hun Joo,[§] Suk Man Cho,[†] Giyoung Song,[†] Sung Hwan Cho,[†] Beomjin Jeong,[†] Ihn Hwang,[†] Jong-Hyun Ahn,[‡] Young-Jun Yu,[⊥] Tae Joo Shin,[¶] Sang Kyu Kwak,[§] Seok Ju Kang,*[,§] and Cheolmin Park*[,†]

[†]Department of Materials Science and Engineering and [‡]School of Electrical and Electronic Engineering, Yonsei University, Seoul 120-749, Korea

[§]School of Energy and Chemical Engineering, Ulsan National Institute of Science and Technology (UNIST), Ulsan 689-798, Korea

[⊥]Creative Research Center for Graphene Electronics, Electronics and Telecommunications Research Institute (ETRI), Daejeon 305-700, Korea

[¶]UNIST Central Research Facilities (UCRF) and School of Natural Science, UNIST 50 UNIST Road, Ulsan 689-798, Korea

S *Supporting Information*

ABSTRACT: Enhancing the device performance of organic memory devices while providing high optical transparency and mechanical flexibility requires an optimized combination of functional materials and smart device architecture design. However, it remains a great challenge to realize fully functional transparent and mechanically durable nonvolatile memory because of the limitations of conventional rigid, opaque metal electrodes. Here, we demonstrate ferroelectric nonvolatile memory devices that use graphene electrodes as the epitaxial growth substrate for crystalline poly(vinylidene fluoride-trifluoroethylene) (PVDF-TrFE) polymer. The strong crystallographic interaction between PVDF-TrFE and graphene results in the orientation of the crystals with distinct symmetry, which is favorable for polarization switching upon the electric field. The epitaxial growth of PVDF-TrFE on a graphene layer thus provides excellent ferroelectric performance with high remnant polarization in metal/ferroelectric polymer/metal devices. Furthermore, a fully transparent and flexible array of ferroelectric field effect transistors was successfully realized by adopting transparent poly[bis(4-phenyl)(2,4,6-trimethylphenyl)amine] semiconducting polymer.

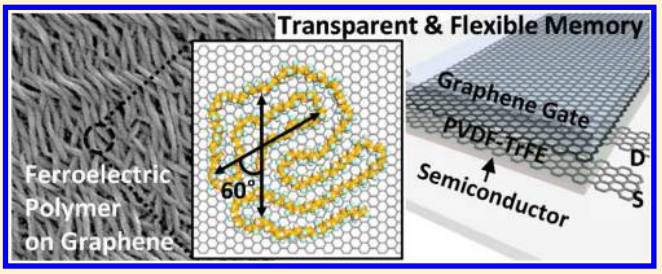

KEYWORDS: *Epitaxial growth, organic memory, ferroelectric polymer, flexible memory, transparent memory*

Solution-processed ferroelectric polymers have been of great interest because of the need to increase the mechanical flexibility and optical transparency of nonvolatile memories. These polymers are being considered as candidates in various organic nonvolatile memory technologies including resistive[1,2] and flash type memories.[3,4] The representative ferroelectric polymer poly(vinylidene fluoride) (PVDF) and its copolymer with trifluoroethylene (TrFE) (PVDF-TrFE) have been successfully employed in two types of memory elements including metal/ferroelectric polymer/metal (MFM) capacitors and ferroelectric field effect transistors (FeFETs).[5−8] In both of these devices, facile rotation of the bistable permanent dipole between hydrogen and fluorine atoms along the polymer chain backbone gives rise to ferroelectric switching of these polymers upon altering the polarity of the applied electric field.[7,8]

Realization of the advantages of the ferroelectric polymers, however, requires careful materials and architecture design of the other memory device components such as semiconductors in a FeFET and electrodes in both FeFETs and MFM capacitors. For instance, both flexible electrodes and flexible semiconductors should be employed to realize a "real" flexible FeFET memory. Previous studies tried to improve aspects of the memory performance of ferroelectric polymer FeFETs including endurance,[9] long data retention,[6] large ON/OFF ratio,[9,10] and scalability.[11] Other studies have focused on imparting new functions including flexibility[5] and printing capability.[10] However, a vexing problem is that these devices present poor optical transparency and undesired surface interactions due to the use of thermally evaporated metals as electrodes (i.e., Al, Au, and Ag). Recently, optically transparent and electrically conductive chemical vapor deposited (CVD) and exfoliated-graphene have been used for organic thin film transistors,[12,13] organic light emitting diodes,[14] floating gated nonvolatile memories,[15] piezoelectric energy generators,[16] organic photovoltaics,[17,18] and nonvolatile ferroelectric polymer memory.[19,20] These graphene films have significant advantages

Received: September 24, 2015
Revised: November 25, 2015

DOI: 10.1021/acs.nanolett.5b03882
Nano Lett. XXXX, XXX, XXX−XXX

such as 97.7% optical transparency and an optimal work function for p-type organic semiconductors. Furthermore, the atomically flat surface of graphene allows for van der Waals epitaxy of organic and inorganic crystals,[21,22] which provides a new way to make tailored crystal orientations and symmetries.

In this work, we investigated the epitaxial growth of PVDF-TrFE films on CVD-graphene electrodes and demonstrated nonvolatile ferroelectric polymer memories. Thin PVDF-TrFE films spin-coated and thermally annealed on graphene were highly crystalline with preferred orientations of both the *b*- and *c*-chain axis aligned parallel to the graphene, which suggests a unique crystallographic interaction between PVDF-TrFE and graphene. A molecular dynamics (MD) simulation further confirmed the strong epitaxial relationship between PVDF-TrFE molecules and the graphene sheet. Using the highly oriented PVDF-TrFE with CVD-graphene electrodes, MFM capacitors exhibited remnant polarization values larger than those with conventional metal electrodes. To demonstrate the suitability of graphene for FeFETs, reactive-ion etching (RIE) and a lift-off process were employed to define three terminal graphene electrodes. The resulting top-gate, bottom contact FeFETs with semiconducting polymer channels were resistant to repetitive mechanical bending as well as folding events with permanent deformation; they also showed good memory performance. Moreover, our graphene-incorporated FeFET became completely transparent when a colorless poly[bis(4-phenyl)(2,4,6-trimethylphenyl)amine] (PTAA) polymer was used as a semiconductor.

The microstructures of the PVDF-TrFE films on a graphene surface were first examined by scanning electron microscopy (SEM). When a PVDF-TrFE film was spin-coated and thermally annealed at 200 °C for 30 min on a SiO_2 layer, the film showed no needle-like structure domains, as shown in Figure 1, panel a.[23,24] In contrast, a unique microstructure of PVDF-TrFE was observed when the film was subsequently melted (200 °C) and recrystallized on the CVD-graphene surface, Figure 1, panel b. The needle-like PVDF-TrFE crystalline domains preferentially grew larger than those from a film annealed at a lower temperature of 135 °C (Supporting Information, Figure S1). Considering that surface morphologies without needle-like crystalline domains have been frequently observed with PVDF-TrFE films on various substrates after recrystallization from a molten state,[7,23] the morphology of the PVDF-TrFE film on graphene surface was unique, and we attributed this to the specific interactions between PVDF-TrFE crystals and the graphene layer.

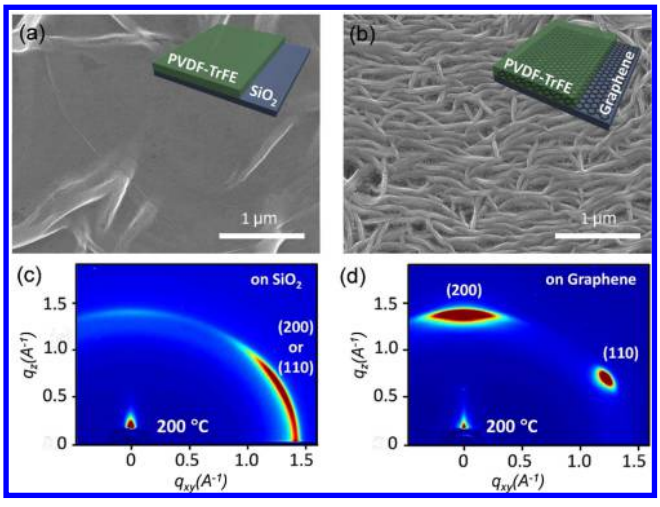

Figure 1. SEM images of 3 wt % PVDF-TrFE on (a) SiO_2 and (b) CVD-graphene substrates thermally annealed at 200 °C for 30 min. The inset presents a schematic of the sample structures. 2D GIXD patterns for 3 wt % PVDF-TrFE films on the (c) SiO_2 and (d) CVD-graphene substrates after thermal annealing at 200 °C for 30 min. Two intensified reflections were observed in the film on a graphene layer in panel d, thus indicating the interaction between PVDF-TrFE crystal and the graphene layer.

To investigate the molecular and crystalline arrangement of a thin PVDF-TrFE film on CVD-graphene, we performed grazing incident X-ray diffraction (GIXD). The crystalline nature of the PVDF-TrFE films exhibited 2D diffraction patterns where a reflection intensified at the meridian regions on the patterns corresponding to either (110) or (200) planes after thermal annealing at 135 °C on SiO_2 and graphene substrates (Supporting Information, Figure S1).[25] It should be noted that the as-spun PVDF-TrFE films also show preferred chain orientation in GIXD patterns mainly arising from the strong centrifugal force during the spin-coating process (Supporting Information, Figure S2).[23] However, the oriented as-spun films need additional thermal annealing process to increase the degree of crystallization for ferroelectric device applications.[23,24] When the film was melted and recrystallized on a SiO_2 substrate, a strong reflection peak arising from either the (110) or (200) plane of the PVDF-TrFE crystals rotated to the equator, as shown in Figure 1, panel c.[23,25] The results show that the *c*-chain axis of PVDF-TrFE crystals preferentially aligned parallel to the surface normal, which is not desirable for ferroelectric polarization switching of a thin PVDF-TrFE film upon electric field, leading to significantly deteriorated polarization performance. However, this detrimental orientation was frequently observed in thin PVDF-TrFE films that were melted and then recrystallized at room temperature on various substrates, making these films hardly suitable for high-temperature processes.[23−25] Interestingly, a melted and recrystallized film on a CVD-graphene layer showed two distinct reflections, which were intensified at the meridian and the region approximately 60 degrees apart from the meridian, as shown in Figure 1, panel d (Supporting Information, Figure S3). This indicated a unique crystallographic interaction between PVDF-TrFE and CVD-graphene, presumably due to the structure and epitaxial registry.

We also fabricated samples with SiO_2/PVDF-TrFE/CVD-graphene as well as exfoliated-graphene/PVDF-TrFE/exfoliated-graphene architecture in which PVDF-TrFE films were covered with either CVD- or exfoliated-graphene layer, and the similar chain orientation to that on the SiO_2/CVD-graphene/PVDF-TrFE structure was also observed in the GIXD pattern and the SEM image for these samples (Supporting Information, Figures S4 and S5). The results imply that the specific crystallographic interaction occurs as long as a PVDF-TrFE film is on contact with a graphene layer or a few graphene layers, allowing for great freedom in fabrication of a nonvolatile memory device involving multistacked layers of the constituents. On the basis of the diffraction patterns and microstructural results in Figure 1, panels a and b, we suggest that the *c*-axis and *a*-axis of the PVDF-TrFE crystals were preferentially oriented parallel and perpendicular to the graphene surface, respectively. Although our experimental results suggest an interesting and specific orientation of PVDF-TrFE crystals on graphene surface, its origin is still unknown mainly due to the

DOI: 10.1021/acs.nanolett.5b03882
Nano Lett. XXXX, XXX, XXX−XXX

polycrystalline nature of a CVD-graphene layer with numerous grain boundaries.

To further investigate the graphene and PVDF-TrFE crystal interactions, we employed mechanically exfoliated-graphene transferred on a SiO_2 substrate. Then, a PVDF-TrFE film was spin-coated onto these layers, and the system was thermally annealed at 200 °C for 30 min. The graphene surface was kept clean before deposition of the PVDF-TrFE film. Figure 2, panel a shows the distinct three-fold symmetry of needle-like PVDF-TrFE crystals on graphene flake (also see Supporting Information, Figure S6). This result clearly indicates that a single grain exfoliated-graphene layer offers a new type of PVDF-TrFE crystal orientation. This unique epitaxial relation between PVDF-TrFE crystal and graphene can be directly visualized by selected area electron diffraction (SAED). For SAED measurement, we transfer a large domain CVD-graphene on amorphous carbon coated transmission electron microscopy (TEM) grid. The resulting SAED pattern in Figure 2, panel b shows that the (001) of PVDF-TrFE crystal with a *d*-spacing of 2.55 Å is highly oriented on graphene surface. One of the main reasons is that the hexagon center-to-center distance of 2.46 Å from graphene sheet shows only 3.7% mismatching of the PVDF-TrFE interchain distance of the *c*-axis (PVDF-TrFE unit cell parameter: a = 9.12 Å, b = 5.25 Å, c = 2.55 Å, β = 93°). This small lattice difference between graphene and PVDF-TrFE suggests that the *c*-axis of PVDF-TrFE crystal follows the zigzag direction of graphene, which enables to induce 30° tilted epitaxial registry in SAED. Previously, we observed epitaxially grown PVDF-TrFE crystals with two-fold symmetry on a mechanically rubbed poly(tetrafluoro ethyelene) (PTFE) surface.[26] Although the epitaxial substrate in the present case is different from rubbed PTFE, we expected that PVDF-TrFE follows similar epitaxial growth on a graphene surface. In addition, epitaxial crystallization of PVDF-TrFE began at the edges of graphene, giving rise to needle-like crystalline domains radiating from the edges of the graphene as shown in Figure 2, panel a.

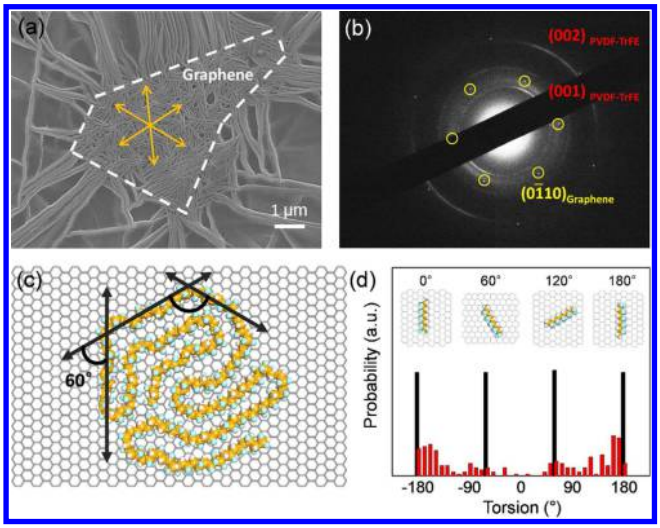

Figure 2. (a) Plane-view SEM image of epitaxial crystallization of 3 wt % PVDF-TrFE films annealed at 200 °C on exfoliated-graphene. The yellow arrows indicate a PVDF-TrFE crystalline lamellae orientation. Three dominant orientations observed on exfoliated-graphene flakes originated from van der Waals surfaces. (b) SAED pattern of oriented PVDF-TrFE (001) plane on the single CVD-graphene layer. The yellow circles indicate the graphene layer. (c) Top view of 100 monomers of PVDF-TrFE on graphene equilibrated using MD simulation. PVDF-TrFE backbones are driven by the preferential adsorption on the atomic lattice of the graphene surface. (d) Plot of the torsional angle (deg) probabilities of initial TG+TG-(black) and final TTTT(red) conformations of PVDF. The PVDF pentamers in the inset show the stable angles with TTTT conformations.

To further elucidate the epitaxy of PVDF-TrFE crystals on graphene, we performed a MD simulation of the organization of PVDF-TrFE molecules on the graphene, as shown in Figure 2, panels c and d. The MD simulation results implied a very strong interaction between PVDF-TrFE and graphene in which a PVDF-TrFE copolymer consisting of 100 monomers with regular alternating VDF trimers and TrFE monomers likely laid on single-layer graphene with its chain axis preferentially aligned along three distinct directions, as shown in Figure 2, panel c. The unique configuration of the polymer chain with 60° rotational symmetry can be further rationalized by the adsorption energy between graphene and PVDF-TrFE. In Figure 2, panel d, the PVDF pentamer with a TTTT conformation had a center of mass located at the center of the graphene. Furthermore, the principal axis of the polymer backbone was aligned parallel to the zigzag direction of graphene. Then, the pentamer was rotated clockwise from 0° to 60° at 10° increments to generate different model systems with unique initial rotation angles. The most stable structures were found to be the pentamers that had a dipole moment parallel to the graphene sheet. Specifically, the lowest adsorption energy was obtained when the backbone was aligned at 0° and 60° along the zigzag direction of graphene (Supporting Information, Figure S7).

Utilization of graphene to develop the oriented PVDF-TrFE crystals allowed us to correlate the crystalline microstructures of PVDF-TrFE films on CVD-graphene with their ferroelectric properties in nonvolatile memory units of both MFM capacitors and FeFETs because the large area CVD-graphene, which also leads to global orientation of a thin PVDF-TrFE film and can serve as an electrode in the devices (Supporting Information, Figure S8). Polarization applied voltage (P–E) hysteresis loops were measured for Al/PVDF-TrFE/graphene capacitors. A CVD-graphene film was transferred onto a highly doped Si substrate.[27,28] Subsequent spin-coating of a PVDF-TrFE film, followed by the deposition of Al top electrodes, allowed us to fabricate a complementary sample set. The capacitors made of Al/PVDF-TrFE/graphene and Al/PVDF-TrFE/highly doped Si are shown in Figure 3, panel a. As expected from SEM and GIXD measurements, a diminished remnant polarization (P_r) value of 4.15 μC/cm^2 was observed for a PVDF-TrFE thin film that was melted and recrystallized on a Si electrode due to the detrimental PVDF-TrFE chain that was orientation toward the electric bias. In contrast, a PVDF-TrFE thin film that was melted and recrystallized on graphene showed a remnant polarization of 6.49 μC/cm^2 and coercive voltage of 17.83 V with a square-like counter-clockwise hysteresis loop. This enhancement of remnant polarization supports our claim that the epitaxial growth of PVDF-TrFE plays a critical role in MFM devices. P–E characteristics of MFMs with different PVDF-TrFE films in thickness are all similar to that of the 3 wt % sample, as summarized in Table 1. From these results, we concluded that graphene is a suitable electrode for high performance ferroelectric capacitors because the epitaxial growth offers the advantage of maintaining a desired PVDF-TrFE orientation after high-temperature treatment. In principle, the remnant polarization value of a PVDF-

DOI: 10.1021/acs.nanolett.5b03882
Nano Lett. XXXX, XXX, XXX−XXX

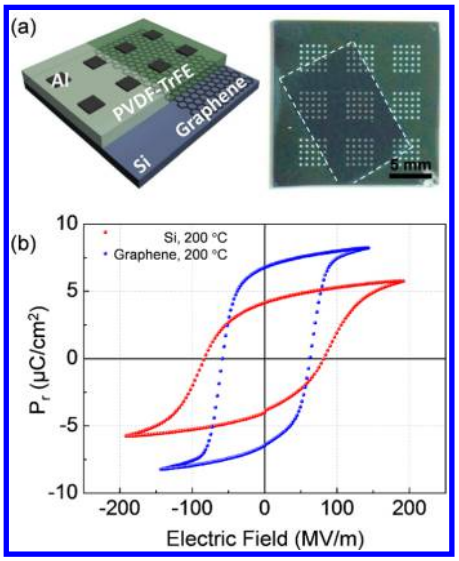

Figure 3. (a) Schematic illustration of the device architecture of an Al/PVDF-TrFE/graphene and Al/PVDF-TrFE/highly doped Si MFM cell (left). Photograph image of a MFM device (right). The white rectangular dots indicate the CVD-graphene layer underneath the PVDF-TrFE film. (b) Polarization versus voltage ($P-V$) curves of ferroelectric PVDF-TrFE thin film.

TrFE film on graphene with long-range crystal orientation is supposed to be even higher than that of a film annealed at 135 °C with polycrystalline domains. The results, however, show that the value on graphene is similar or slightly lower than that of a film annealed at 135 °C. One of the reasons may be the thickness of a PVDF-TrFE film employed to the MFM capacitor. In our polarization measurement setup, a PVDF-TrFE film with the minimum film thickness of approximately 100 nm is required to avoid electrical leakage problem. Considering that a critical film thickness above which epitaxial crystal interaction begins to diminish is approximately 50 nm in the most epitaxial polymer films, the contribution of the epitaxially grown PVDF-TrFE crystals to the overall polarization performance becomes marginal in our experimental conditions.

To confirm our speculation, we characterized surface morphology of a PVDF-TrFE film on graphene as a function of film thickness. Highly ordered epitaxial crystalline structure disappeared when a film was approximately 500 nm above (>5 wt %) which edge-on crystal domains are still developed with the preferred *c*-axis crystal orientation but with many structural defects (Supporting Information, Figure S9). When a film is thicker than approximately 2000 nm, the morphology becomes identical to that developed on a Si substrate, indicative of no longer epitaxial interaction remaining on the surface of the PVDF-TrFE film. GIXD results of the PVDF-TrFE films on graphene as a function of film thickness also support the morphological data (Supporting Information, Figure S10). Despite the slightly lower remnant polarization, our epitaxial PVDF-TrFE film is still beneficial for high-temperature processes.

CVD-graphene electrodes exhibit unique optical transparency as well as mechanical flexibility.[27] To take advantage of these properties, we employed FeFETs with PVDF-TrFE films to fabricate multifunctional transistor-type nonvolatile memories. Fabrication of a functional FeFET with either optical transparency or mechanical flexibility requires all source, drain, and gate electrodes be made of CVD-graphene. Furthermore, depending upon the functionality, semiconducting channel layers should be transparent or flexible. We, therefore, developed an elaborate device fabrication process that included several film transfer and RIE etching steps as schematically shown in Figure 4. CVD-graphene with poly(methyl methacrylate) (PMMA) supporting layer was transferred onto a mechanically flexible poly(ethylene terephthalate) (PET)/poly(4-vinylphenol) substrate, followed by removal of the PMMA layer. It is noted that the PVDF-TrFE crystal orientation is rarely affected by the presence of the PMMA residue, which frequently remains after the graphene transfer with a PMMA supporting layer on graphene surface

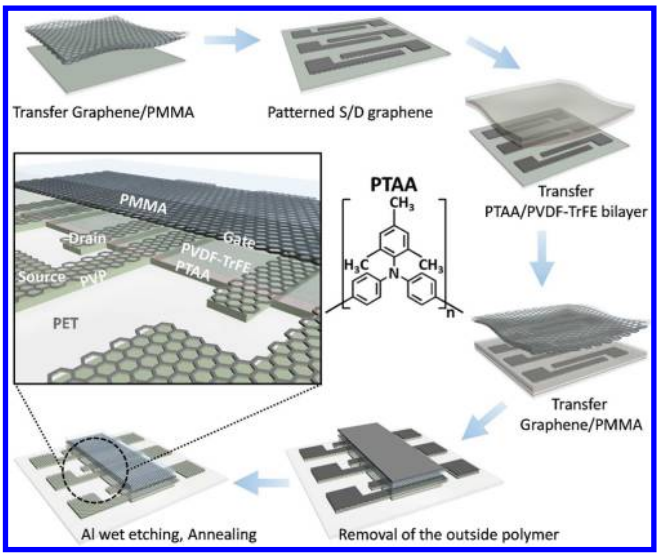

Figure 4. Schematic presentation of the FeFET device fabrication process. A fully transparent and flexible PVDF-TrFE FeFET was fabricated by stacking a transparent PTAA semiconductor, graphene electrodes, and the PVDF-TrFE dielectric with conventional transfer and RIE etching steps.

Table 1. Device Performance of MFM Capacitors with Various Thicknesses and Various Annealing Temperatures on Si or CVD-Graphene Substrates

	Si		graphene			
temperature	135 °C	200 °C	135 °C	200 °C		
concentration	3 wt %	3 wt %	3 wt %	2 wt %	3 wt %	5 wt %
P_r (μC/cm^2)	7.30	4.15	7.23	6.77	6.49	6.14
V_c (MV/m)	66.28	83.98	63.58	74.43	73.16	69.48
P_{sat} (μC/cm^2)	8.83	5.75	8.75	8.16	7.87	7.44
thickness (nm)	288.14	260.76	301.94	117.28	243.68	558.42

DOI: 10.1021/acs.nanolett.5b03882
Nano Lett. XXXX, XXX, XXX−XXX

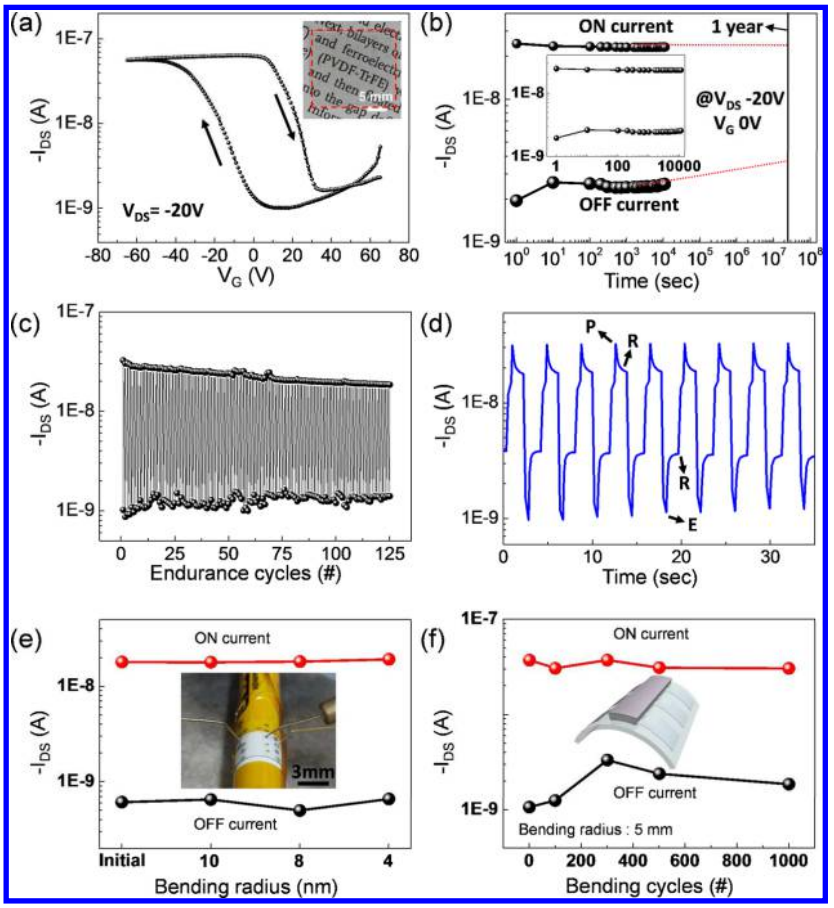

Figure 5. (a) $I_{DS}-V_G$ transfer characteristics of PTAA channel FeFET. The inset shows a photograph of the transparent FeFETs. The red rectangular dots indicate the FeFETs employing a PET/PVP/CVD-graphene/PTAA/PVDF-TrFE/CVD-graphene/PMMA architecture. (b) Data retention characteristics of a FeFET memory measured with the ON and OFF state drain currents. The red dots indicate extrapolation of both ON and OFF current. (c) The time-dependent write/erase endurance cycles of drain current. (d) I_{DS} dynamics with V_G sequence program (P)-read (R)-erase (E)-read (R) (±60 V, 50 ms pulse width) at V_{DS} = −20 V. On and off currents of a flexible FeFET device with a PTAA channel as a function of (e) bending radius and (f) the number of bending cycles.

(Supporting Information, Figure S11). Arrays of patterned graphene source and drain electrodes were fabricated by selective etching of the graphene by RIE through a 25 nm thick Al pattern mask that had been thermally evaporated on the graphene.[29] A bilayer of semiconducting poly[bis(4-phenyl)-(2,4,6-trimethylphenyl)amine] (PTAA) and ferroelectric PVDF-TrFE was prepared by sequential spin-coatings with orthogonal solvents,[30] and this bilayer was subsequently transferred to the prepatterned source and drain electrodes, as shown in Figure 4. Next, another graphene/PMMA layer was transferred onto the PVDF-TrFE layer for top gate fabrication. A 70 nm thick Al film was thermally evaporated through a shadow mask onto the graphene/PMMA layer. This was followed by RIE etching, which removed both the PVDF-TrFE and semiconducting polymer located in the areas not covered by the Al pattern mask. Finally, the residual Al on the graphene electrodes was removed using an ammonium persulfate solution, giving rise to a FeFET with graphene source, drain, and gate electrodes as shown in Figure 4. It should be noted that the supporting PMMA layer on the graphene gate electrode still remained after the final step, but this did not influence transparency or flexibility.

Nonvolatile memory performances of our FeFETs with all graphene three terminal electrodes were examined, and the results are shown in Figure 5. A FeFET with a PTAA semiconductor exhibited a characteristic $I_{DS}-V_G$ transfer hysteresis curve arising from ferroelectric switching of the PVDF-TrFE gate insulator upon V_G sweep as shown in Figure 5, panel a. The arrays of FeFETs with graphene electrodes were optically transparent, particularly when a transparent PTAA semiconducting layer was employed as shown in the inset of Figure 5, panel a. The optical transparency of our FeFET was further quantified by UV−vis spectroscopy (Supporting Information, Figure S12). As expected, the transmittance of the multilayers including PTAA was 90% of the value of PET. The absolute transmittance was greater than 84% for the stacked films over the whole visible range.

Our device exhibited excellent time dependent data retention as well as write/read cycle endurance properties as shown in Figure 5, panels b and c, respectively. On and off currents independently measured at zero V_G with a V_{DS} of −20 V hardly changed over times longer than 10^4 s as shown in the inset of Figure 5, panel b. Extrapolation of both on and off current with time suggests that a decent current margin remained even after a year. For repetitive data programing and erasing, the cycle endurance of a device based on a gate voltage sweep (sequence of erase/read/program/read steps) was examined, and the results in Figure 5, panel c show that the on/off current ratio was well maintained even after more than 10^2 cycles. The dynamic property of I_{DS} upon program/read/erase/read

DOI: 10.1021/acs.nanolett.5b03882
Nano Lett. XXXX, XXX, XXX−XXX

sequences was investigated with time as shown in Figure 5, panel d. The device was successfully switched from on to off at a time interval of 50 ms.

Our FeFETs with all graphene source, drain, and gate electrodes are not only optically transparent, but also mechanically flexible. The nonvolatile memory performance of a FeFET under various mechanical stimuli was systematically examined as a function of bending radius as well as number of bending cycles as shown in Figure 5, panels e and f, respectively. The initial on and off current of a FeFET in a flat state was hardly changed when bent with various bending radius down to 4 mm. Both on and off current values of the device bent at a radius of 5 mm were well maintained even after 1000 repetitive bending cycles as shown in Figure 5, panel f. For further mechanical deformation, arrays of FeFETs with graphene electrodes were carefully folded along the center of the common gate electrode. The experimental results demonstrate that the FeFETs work properly even under severe folding deformation (Supporting Information, Figure S13). We compared the device performance of our flexible and transparent FeFETs with the previous memories (Supporting Information, Figure S14). The current work clearly represents that our novel memory with graphene electrodes is one of the most transparent as well as mechanically flexible devices and exhibits its device performance very comparable with those of the previously reported ones.

In conclusion, we demonstrated the fabrication of highly transparent and flexible ferroelectric memory devices using CVD-graphene as electrodes for both MFM and FeFETs. By employing mechanically exfoliated single and a few layers graphene, combined with MD simulation, we showed that epitaxial growth of PVDF-TrFE crystals was successfully achieved on the 2D crystal surface with the characteristic three-fold symmetry. The orientation of the epitaxial crystals on graphene was favorable for polarization switching upon the electric field regardless of the processing temperature, giving rise to the higher ferroelectric performance in MFM devices. Furthermore, a transparent PTAA semiconducting layer with CVD-graphene electrodes enabled us to produce highly transparent and mechanically flexible FeFETs that potentially open up new opportunities in the field of organic transparent electronics.

■ ASSOCIATED CONTENT

Supporting Information

The Supporting Information is available free of charge on the ACS Publications website at DOI: 10.1021/acs.nanolett.5b03882.

Experimental section; supporting figures (PDF)

■ AUTHOR INFORMATION

Corresponding Authors

*E-mail: sjkang@unist.ac.kr.
*E-mail: cmpark@yonsei.ac.kr.

Author Contributions

The manuscript was written through contributions of all authors. All authors have given approval to the final version of the manuscript.

Notes

The authors declare no competing financial interest.

■ ACKNOWLEDGMENTS

This research was supported by a grant from the National Research Foundation of Korea (NRF), funded by Korean government (MEST) (No. 2014R1A2A1A01005046) and by Global Ph.D Fellowship Program through the NRF funded by the Ministry of Education (NRF-2014H1A2A1021571). This work was supported (in part) by the Yonsei University Yonsei-SNU Collaborative Research Fund of 2014. S.J.K. was supported by the Research Fund of the UNIST in 2015 (1.150119.01). This research was supported by Basic Science Research Program through the NRF funded by the Ministry of Education (NRF-2015R1D1A1A02060332). S.K.K. acknowledges a fund from NRF-2014M1A8A1049255 and computational resources from UNIST-HPC and KISTI-PLSI. The authors especially thank Hyeong Joo Choi, who has developed the data acquisition system and data processing software. The authors also acknowledge Hoju Kang, who has helped GIXD experiments. Experiments at PLS-II 6D UNIST-PAL beamline were supported in part by MEST, POSTECH, and UNIST UCRF.

■ REFERENCES

(1) Cho, B.; Song, S.; Ji, Y.; Kim, T.-W.; Lee, T. *Adv. Funct. Mater.* **2011**, *21*, 2806−2829.
(2) Hwang, S. K.; Lee, J. M.; Kim, S.; Park, J. S.; Park, H. I.; Ahn, C. W.; Lee, K. J.; Lee, T.; Kim, S. O. *Nano Lett.* **2012**, *12*, 2217−2221.
(3) Baeg, K.-J.; Khim, D.; Kim, D.-Y.; Jung, S.-W.; Koo, J. B.; Noh, Y.-Y. *Jpn. J. Appl. Phys.* **2010**, *49*, 05EB01.
(4) Singh, T. B.; Marjanović, N.; Matt, G. J.; Sariciftci, N. S.; Schwödiauer, R.; Bauer, S. *Appl. Phys. Lett.* **2004**, *85*, 5409−5411.
(5) Hwang, S. K.; Bae, I.; Kim, R. H.; Park, C. *Adv. Mater.* **2012**, *24*, 5910−5914.
(6) Naber, R. C. G.; Tanase, C.; Blom, P. W. M.; Gelinck, G. H.; Marsman, A. W.; Touwslager, F. J.; Setayesh, S.; de Leeuw, D. M. *Nat. Mater.* **2005**, *4*, 243−248.
(7) Park, Y. J.; Bae, I.-S.; Kang, S. J.; Chang, J.; Park, C. *IEEE Trans. Dielectr. Electr. Insul.* **2010**, *17*, 1135−1163.
(8) Naber, R. C. G.; Asadi, K.; Blom, P. W. M.; de Leeuw, D. M.; de Boer, B. *Adv. Mater.* **2010**, *22*, 933−945.
(9) Zaitsu, K.; Lee, S.; Ishibe, K.; Sekitani, T.; Someya, T. *J. Appl. Phys.* **2010**, *107*, 114506.
(10) Sekitani, T.; Zaitsu, K.; Noguchi, Y.; Ishibe, K.; Takamiya, M.; Sakurai, T.; Someya, T. *IEEE Trans. Electron Devices* **2009**, *56*, 1027−1035.
(11) Naber, R. C. G.; de Boer, B.; Blom, P. W. M.; de Leeuw, D. M. *Appl. Phys. Lett.* **2005**, *87*, 203509.
(12) Kang, S. J.; Lee, G.-H.; Yu, Y.-J.; Zhao, Y.; Kim, B.; Watanabe, K.; Taniguchi, T.; Hone, J.; Kim, P.; Nuckolls, C. *Adv. Funct. Mater.* **2014**, *24*, 5157−5163.
(13) Lee, W. H.; Park, J.; Sim, S. H.; Jo, S. B.; Kim, K. S.; Hong, B. H.; Cho, K. *Adv. Mater.* **2011**, *23*, 1752−1756.
(14) Han, T.-H.; Lee, Y.; Choi, M.-R.; Woo, S.-H.; Bae, S.-H.; Hong, B. H.; Ahn, J.-H.; Lee, T.-W. *Nat. Photonics* **2012**, *6*, 105−110.
(15) Bertolazzi, S.; Krasnozhon, D.; Kis, A. *ACS Nano* **2013**, *7*, 3246−3252.
(16) Choi, D.; Choi, M.-Y.; Choi, W. M.; Shin, H.-J.; Park, H.-K.; Seo, J.-S.; Park, J.; Yoon, S.-M.; Chae, S. J.; Lee, Y. H.; Kim, S.-W.; Choi, J.-Y.; Lee, S. Y.; Kim, J. M. *Adv. Mater.* **2010**, *22*, 2187−2192.
(17) Wang, Y.; Chen, X.; Zhong, Y.; Zhu, F.; Loh, K. P. *Appl. Phys. Lett.* **2009**, *95*, 063302.
(18) Gomez De Arco, L.; Zhang, Y.; Schlenker, C. W.; Ryu, K.; Thompson, M. E.; Zhou, C. *ACS Nano* **2010**, *4*, 2865−2873.
(19) Zheng, Y.; Ni, G.-X.; Toh, C.-T.; Zeng, M.-G.; Chen, S.-T.; Yao, K.; Özyilmaz, B. *Appl. Phys. Lett.* **2009**, *94*, 163505.
(20) Bae, S.-H.; Kahya, O.; Sharma, B. K.; Kwon, J.; Cho, H. J.; Özyilmaz, B.; Ahn, J.-H. *ACS Nano* **2013**, *7*, 3130−3138.

DOI: 10.1021/acs.nanolett.5b03882
Nano Lett. XXXX, XXX, XXX−XXX

(21) Lee, C.-H.; Schiros, T.; Santos, E. J. G.; Kim, B.; Yager, K. G.; Kang, S. J.; Lee, S.; Yu, J.; Watanabe, K.; Taniguchi, T.; Hone, J.; Kaxiras, E.; Nuckolls, C.; Kim, P. *Adv. Mater.* **2014**, *26*, 2812−2817.
(22) Lee, W. C.; Kim, K.; Park, J.; Koo, J.; Jeong, H. Y.; Lee, H.; Weitz, D. A.; Zettl, A.; Takeuchi, S. *Nat. Nanotechnol.* **2015**, *10*, 423−428.
(23) Park, Y. J.; Kang, S. J.; Park, C.; Kim, K. J.; Lee, H. S.; Lee, M. S.; Chung, U.-I.; Park, I. J. *Appl. Phys. Lett.* **2006**, *88*, 242908.
(24) Mao, D.; Quevedo-Lopez, M. A.; Stiegler, H.; Gnade, B. E.; Alshareef, H. N. *Org. Electron.* **2010**, *11*, 925−932.
(25) Lee, J. S.; Prabu, A. A.; Kim, K. J. *Polymer* **2010**, *51*, 6319−6333.
(26) Park, Y. J.; Kang, S. J.; Lotz, B.; Brinkmann, M.; Thierry, A.; Kim, K. J.; Park, C. *Macromolecules* **2008**, *41*, 8648−8654.
(27) Li, X.; Zhu, Y.; Cai, W.; Borysiak, M.; Han, B.; Chen, D.; Piner, R. D.; Colombo, L.; Ruoff, R. S. *Nano Lett.* **2009**, *9*, 4359−4363.
(28) Li, X.; Cai, W.; An, J.; Kim, S.; Nah, J.; Yang, D.; Piner, R.; Velamakanni, A.; Jung, I.; Tutuc, E.; Banerjee, S. K.; Colombo, L.; Ruoff, R. S. *Science* **2009**, *324*, 1312−1314.
(29) Kang, B.; Lim, S.; Lee, W. H.; Jo, S. B.; Cho, K. *Adv. Mater.* **2013**, *25*, 5856−5862.
(30) Asadi, K.; Blom, P. W. M.; de Leeuw, D. M. *Appl. Phys. Lett.* **2011**, *99*, 053306.

DOI: 10.1021/acs.nanolett.5b03882
Nano Lett. XXXX, XXX, XXX−XXX